Crystal Structure and Solid-State Properties of 3,4-Diaminopyridine Dihydrogen Phosphate and Their Comparison with Other Diaminopyridine Salts

ARTICLE *in* CRYSTAL GROWTH & DESIGN · FEBRUARY 2013

Impact Factor: 4.89 · DOI: 10.1021/cg3014249

CRYSTAL GROWTH & DESIGN

Article

pubs.acs.org/crystal

Crystal Structure and Solid-State Properties of 3,4-Diaminopyridine Dihydrogen Phosphate and Their Comparison with Other Diaminopyridine Salts

Nathalie Mahé,[†] Béatrice Nicolaï,[†] Hassan Allouchi,[‡] Maria Barrio,[§] Bernard Do,[∥,⊥] René Céolin,[†,§] Josep-Lluis Tamarit,[§] and Ivo B. Rietveld*[,†]

[†]EAD Physico-chimie Industrielle du Médicament (EA4066), Faculté de Pharmacie, Université Paris Descartes, 4, Avenue de l'Observatoire, 75006 Paris, France

[‡]Recherche et Innovation en Chimie Médicinale (RICM, ISP-UMR 1282), Faculté de Pharmacie, Université François Rabelais, 31 Avenue Monge, 37200 Tours, France

[§]Grup de Caracterització de Materials (GCM), Departament de Fisica i Enginyeria Nuclear, Universitat Politécnica de Catalunya, ETSEIB, Diagonal 647, 08028 Barcelona, Spain

[∥]Etablissement Pharmaceutique de l'Assistance Publique-Hôpitaux de Paris, Agence Générale des Equipements et Produits de Santé, 7, rue du Fer á Moulin, 75005 Paris, France

[⊥]Chimie Analytique, Faculté de Pharmacie, Université Paris Descartes, 4, Avenue de l'Observatoire, 75006 Paris, France

Supporting Information

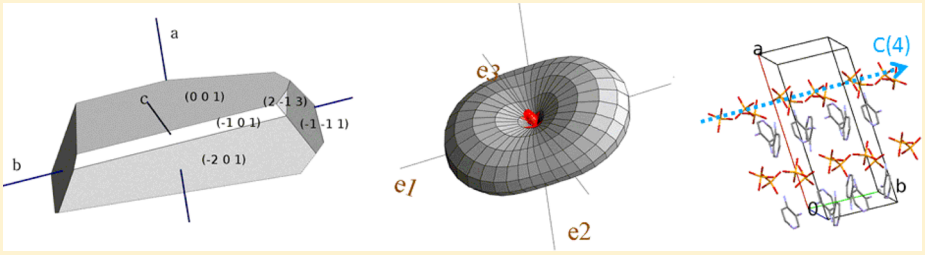

ABSTRACT: 3,4-Diaminopyridine is an active pharmaceutical ingredient for the treatment of Lambert–Eaton myasthenic syndrome (LEMS). It is 3,4-diaminopyridine dihydrogen phosphate that has become the active ingredient of choice. As part of a larger study for the development of this drug, solid-state studies have been carried out. At room temperature, the crystals are monoclinic ($C2/c$). Dihydrogen phosphate anions $H_2PO_4^-$ form infinite chains parallel to the b axis, and these chains can be considered as macroanions $(H_2PO_4)\infty$. The organic cations form hydrogen bonds with the macroanions bridging them together. A negative thermal expansion is observed along the [103] direction in the crystal, which coincides with the direction of chains of interchanging anions and cations. The crystal packing shows similarities with the hydrogen tartrate salt as illustrated by a Hirshfeld surface analysis. This phosphate and this tartrate salt are also the two diaminopyridine salts that have been selected for therapeutic use because of their appropriate physical properties.

INTRODUCTION

3,4-Diaminopyridine ($C_5H_7N_3$, cf. Figure 1; from here on, 3,4-DAP) is an efficient drug to treat muscular weakness caused by the Lambert–Eaton myasthenic syndrome (LEMS) first described by Lambert, Eaton, and Rooke in 1956.[1−7] It has been shown to block the voltage-dependent K-channels;[5,8] however, the molecule is too unstable for commercialization.[6,7,9] Six 3,4-DAP salts have been produced with counterions in accordance with FDA regulations (hydrogen chloride, hydrogen bromide, sulfate, dihydrogen phosphate, tartrate, and benzoate).[7,8] These salts are more stable than the molecule itself; the involvement of the lone electron pair on the pyridine nitrogen in a charge-assisted hydrogen bond reduces the possibility of oxidation for 3,4-DAP.[7,9] Among the six salts, only two (dihydrogen phosphate and hydrogen tartrate) have been selected for medical use because they appear physically and chemically stable in time, possess little hygroscopicity, have excellent solubility in water, and have an acceptable pH in saturated solution.[7]

Physical–chemical stability and bioavailability are strongly influenced by the crystalline form of a substance.[10] A survey of the literature demonstrated that a number of crystal structures of 3,4-DAP salts have been determined together with the structure of the free base.[11] Crystal structures involving the cation $3,4\text{-DAPH}^+$ (Figure 1) include dinitrosalicylate,[12] hydrogen squarate,[13] hydrogen succinate,[14] 4-nitro-benzoate-

Received: September 28, 2012
Revised: December 13, 2012
Published: December 21, 2012

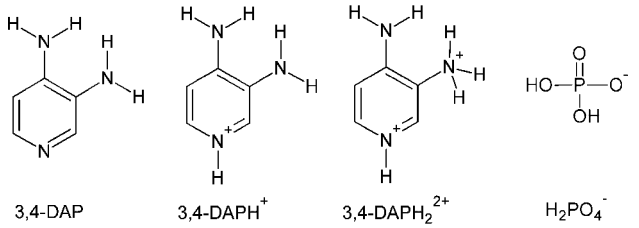

Figure 1. Molecular structure of 3,4-diaminopyridine (3,4-DAP), the protonated 3,4-diaminopyridine cation (3,4-DAPH$^+$), the diprotonated 3,4-diaminopyridine cation (3,4-DAPH$_2^{2+}$), and the dihydrogen phosphate anion ($H_2PO_4^-$).

4-nitrobenzoic acid,[15] and hydrogen tartrate dehydrate.[16] Other solved structures contain the diprotonated cation 3,4-DAPH$_2^{2+}$ (Figure 1): dichloride,[17] dinitrate,[18] and bis(perchlorate) salts.[19] However, the structure of the dihydrogen phosphate salt ($C_5H_8N_3{\cdot}H_2PO_4$, from here on, 3,4-DAPH$^+{\cdot}H_2PO_4^-$; cf. Figure 1), which is used therapeutically and is even patented together with the tartrate salt,[6] had not been determined up until 2011, when its structure was solved and found to be monoclinic (space group $I2/c$) by Le Bail and Smrčok from high-resolution powder diffraction.[20] As part of a larger study for the development of 3,4-DAPH$^+{\cdot}H_2PO_4^-$,[7] solid-state studies of this active pharmaceutical ingredient (API) have been carried out. It resulted in the determination of the crystal structure from a single crystal, which has been compared to the published structures of the 3,4-DAP salts.

MATERIALS AND METHODS

Sample Preparation. A crystalline powder of 3,4-diaminopyridine dihydrogen phosphate ($C_5H_8N_3{\cdot}H_2PO_4$, M = 207.13 g mol^{-1}) of medicinal grade was obtained from SERATEC (France). Crystals were grown by vapor diffusion; the compound was dissolved in a small quantity of water, and solvent vapor of acetonitrile was slowly allowed to diffuse into the aqueous solution at room temperature resulting in the formation of long, thin needles attached to each other in the form of sea urchins.

Single Crystal X-ray Diffraction. X-ray diffraction data were collected at 296 K on an X-CALIBUR-2 CCD 4-circle diffractometer (Oxford Diffraction) with graphite-monochromated Mo$K\alpha$ radiation (λ = 0.71073 Å). Data reduction including interframe scaling, Lorentz polarization, empirical absorption, and detector sensitivity corrections were carried out using CrysAlis software (Oxford Diffraction).[21] Crystal data and selected refinement details are summarized in Table 1. Structures were solved by direct methods and subsequently refined by a full matrix least-squares method on F^2 using SHELX.[22] Non-hydrogen atoms were refined with anisotropic thermal parameters. All H-atoms were located in a difference Fourier map and allowed to refine freely. Short contacts were analyzed using PLATON.[23] Supplementary crystallographic data can be found in the Cambridge Crystallographic Data Centre free of charge via www.ccdc.cam.ac.uk/data_request/cif/; CCDC ID 884960.

Differential Scanning Calorimetry. Thermogravimetry (TGA) was carried out at various rates with a TGA50 thermobalance from TA-Instruments. Differential scanning calorimetry (DSC) experiments were run at various heating rates with a Q100 thermal analyzer from TA-Instruments (New Castle, DE, USA) calibrated with indium (T_{fus} = 429.75 K; $\Delta_{fus}H$ = 3.267 kJ mol^{-1}) as standard for temperature and enthalpy. Specimens were weighed with a balance sensitive to 0.01 mg.

High-Resolution X-ray Powder Diffraction As a Function of Temperature. X-ray powder diffraction was carried out on a transmission mode diffractometer using Debye–Scherrer geometry equipped with a cylindrical position-sensitive detector (CPS120) from INEL (France) containing 4096 channels (0.029° 2θ angular step) with monochromatic Cu–Kα_1 (λ = 1.5406 Å) radiation. For the measurements as a function of temperature, a liquid nitrogen 700 series Cryostream Cooler from Oxford Cryosystems (Oxford, U.K.) was used.

Ground specimens were introduced in a Lindemann capillary (0.5 mm diameter) rotating perpendicularly to the X-ray beam during the experiments to improve the average over the crystallite orientations. For the temperature dependent measurements in the range from 100 K up to the melting point, the sample temperature was equilibrated for about 10 min followed by an acquisition time of ca. 1 h. The heating rate in between data collection was 1.33 K min^{-1}.

Isobaric Thermal Expansion Tensor. The anisotropy of the intermolecular interactions can be investigated with the isobaric thermal expansion tensor, which is a measure for how the interactions change with temperature.[24] The expansion tensor has been calculated with the DEFORM program:[25] it is a symmetrical second-rank tensor, with nonzero eigenvalues on the diagonal α_{11}, α_{22}, and α_{33} on the basis of the eigenvectors **e1**, **e2**, and **e3**. A small value for a tensor eigenvalue is commonly referred to as a hard direction, because it indicates a small deformation, and a large value as a soft direction, because it indicates a large deformation.[26−30] The anisotropy of the thermal expansion can be expressed as a single value by the aspherism coefficient, comprising the three coefficients of the thermal tensor.[26−28,30,31] The vast majority of solids expand when heated because of the anharmonic nature of the chemical bond potential. Some materials display negative thermal expansion, that is lattice contraction with increasing temperature in one, two, or even in all directions.

Hirshfeld Surfaces and Fingerprint Plots. The analysis of molecular interactions in a crystal through Hirshfeld surfaces is increasingly used for solid-state characterization of pharmaceutical materials.[29,30,32,33] Hirshfeld surface calculations were performed with Crystal Explorer[34] using experimental crystal geometries as input. A Hirshfeld surface encloses the molecular volume based on the electron density difference with the average value of the crystal. It can be mapped with various functions such as curvedness[35] or electrostatic potential.[36] Distance d_i is defined as the distance from the Hirshfeld surface to the nearest interior atom and d_e is the distance from the

Table 1. Crystal and Refinement Data for 3,4-Diaminopyridine Dihydrogen Phosphate

molecular formula	$C_5N_3O_4H_{10}P$
formula weight	207.13 g/mol
CCDC no.	884960
crystal system	monoclinic
space group	$C2/c$
unit cell dimension	a = 20.3871(13) Å
	b = 7.7263(2) Å
	c = 14.6064(9) Å
	β = 128.494(10) °
volume (Å^3)	1800.7(3)
Z	8
T (K)	296(2)
calculated density (g/cm^3)	1.528
absorption coefficient (mm^{-1})	0.294
F(000)	864
color, habit	needle colorless
crystal size (mm)	0.335 × 0.100 × 0.100
θ range for data collection (deg)	2.9231−31.5407
index ranges	$-29 \le h \le 29$; $-11 \le k \le 10$; $-21 \le l \le 20$
reflections collected/unique	18604/2837
data/parameters/restraints	2837/158/0
goodness-of-fit on F^2	0.964
Final R indices [$I > 2\sigma(I)$]	0.0367
largest diff. peak and hole (e/Å^3)	0.403 and −0.211

dx.doi.org/10.1021/cg3014249 | Cryst. Growth Des. 2013, 13, 708−715

surface to the nearest exterior atom.[37] Plots of d_e against d_i, called fingerprint plots, offer the possibility to classify crystals by the nature of their intermolecular interactions and to rapidly identify similarities.[28,37,38]

RESULTS AND DISCUSSION

Calorimetric Data for 3,4-DAPH$^+$·$H_2PO_4^-$. The melting point of 3,4-DAPH$^+$·$H_2PO_4^-$ was found at 512.9 K with a melting enthalpy of 218.4 J g^{-1}. Because there were indications of decomposition during the melt, TGA measurements were carried out. The weight loss during the melt was 2.5%, and in addition, the baseline after the melt as determined by DSC in a closed pan is only slightly higher than before the melt (Figure 2). This means that the estimate for the enthalpy of fusion is

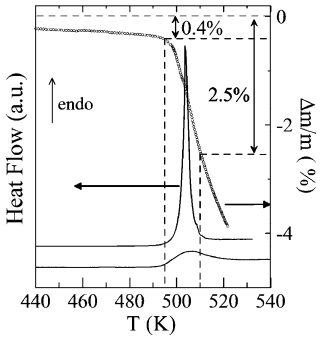

Figure 2. Melting peak of 3,4-diaminopyridine dihydrogen phosphate by DSC with the weight loss overlay obtained by TGA at 10 K/min. Left hand axis, heat flow as determined by DSC, and right-hand axis, relative weight loss of the sample by TGA. The line below the DSC curve is the derivative of the weight loss curve as a function of temperature.

most likely close to the real value. At the onset temperature, no significant weight loss has occurred; therefore, it can be concluded that the onset temperature of the melting event is not affected by decomposition.

Crystal Structure and Proton Transfer. 3,4-Diaminopyridine dihydrogen phosphate crystallizes in the monoclinic space group $C2/c$ with room temperature lattice parameters a = 20.3871(13) Å, b = 7.7263(2) Å, c = 14.6064(9) Å, and β = 128.494(10)°. The unit-cell volume is 1800.7(3) Å^3 containing Z = 8 formula units. The asymmetric unit consists of one protonated 3,4-diaminopyridine cation (3,4-DAPH$^+$) and one dihydrogen phosphate anion $H_2PO_4^-$ (Figure 3 and Table S1, Supporting Information). The protonation of the N1 atom leads to an increase of the C1−N1−C5 angle (121.47(2)°) with respect to the value found in the structure of neutral 3,4-

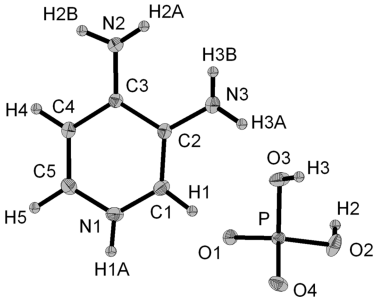

Figure 3. ORTEP plot of 3,4-diaminopyridine dihydrogen phosphate with atom numbering.

DAP (115.69(19)°).[11] The same effect is observed in the published structures with 3,4-DAPH$^+$ and 3,4-DAPH$_2^{2+}$.[12,17,18]

Comparison with the Structure Found by Le Bail and Smrčok. A comparison of the X-ray powder diffraction profiles calculated with the crystal structures from Le Bail and Smrčok[20] and from the present study demonstrates that the profiles are virtually one and the same. They also coincide with the experimental diffraction profile obtained in this study. It demonstrates that the structure found from powder diffraction and that from single crystal diffraction are identical even though different unit cells have been chosen. Both findings obviously belong to the same monoclinic space group that can be described using the standard setting $C2/c$ (this work) or the nonstandard setting $I2/c$. The latter is a consequence of the choice of the shortest lattice parameters and a β angle closest to 90°. The transformation matrix to change from one to the other unit cell is given in the Supporting Information.

Further comparison indicates that the structure found by Le Bail and Smrčok, although less accurate, is fully confirmed by the present work. In particular, calculations carried out by Le Bail and Smrčok indicated that a hydrogen atom belonging to phosphoric acid is bound to the nitrogen of the pyridine ring, which has been experimentally observed in the present work as mentioned above.[20]

Molecular Geometry. The aromatic ring of the protonated 3,4-diaminopyridine cation is planar, with a maximum deviation of 0.0185 (10) Å for atom C3. The 4 hydrogen atoms of the two NH_2 groups are slightly out of the molecular plane as found for the majority of the crystal structures of the other 3,4-DAPH$^+$ salts[12,14−16] as well as for the geometry of the isolated 3,4-DAPH$^+$ cation calculated with several ab initio methods.[39,40]

Distances and angles found in the experimental geometry of 3,4-DAPH$^+$ are consistent with those found in the crystal structures of other 3,4-DAPH$^+$ salts. It can be seen that the C−N bond lengths in the meta and para position in relation to N1 (Table S1, Supporting Information) are different; the electronic resonance that stabilizes the pyridinium cation is shared by N2, which is sp^2 hybridized, whereas N3 is sp^3 hybridized.

In the tetrahedral dihydrogen phosphate anion, the protonated P−O vertices (O2 and O3) are found at an increased distance from the phosphor atom (Table S1, Supporting Information) relative to the P−O bonds involving O1 and O4. The bond lengths are in good agreement with those observed in anions of similar phosphates.[41−43]

Intermolecular Interactions. The aromatic rings of neighboring 3,4-DAPH$^+$ moieties are involved in antiparallel $\pi\cdots\pi$ interactions (Figure 4) with an interplanar distance of 3.36 Å consistent with the interplanar distances found in several other 3,4-DAPH$^+$ salts with antiparallel $\pi\cdots\pi$ interactions (3.31 Å in the tartrate[16] and the succinate salt[14] and 3.35 Å in the squarate salt[13]).

A complex 3D network exists consisting of intermolecular N−H···O hydrogen bonds between the organic cation and the surrounding dihydrogen phosphate anions. In addition, the phosphate ions are interconnected by O−H···O hydrogen bonds (Figure 4). This gives rise to a three-dimensional supramolecular array of $H_2PO_4^-$ groups encapsulating the organic moieties in columns. In these columns, the infinite chains of antiparallel $\pi\cdots\pi$ interactions are located (Figure 4b).

The $H_2PO_4^-$ units form cyclic dimers, graph set assignment $R_2^2(8)$, and infinite chains C(4) propagating along the b axis (Figures 4a,c and Table 2). The O−H···O hydrogen bond is

dx.doi.org/10.1021/cg3014249 | Cryst. Growth Des. 2013, 13, 708−715

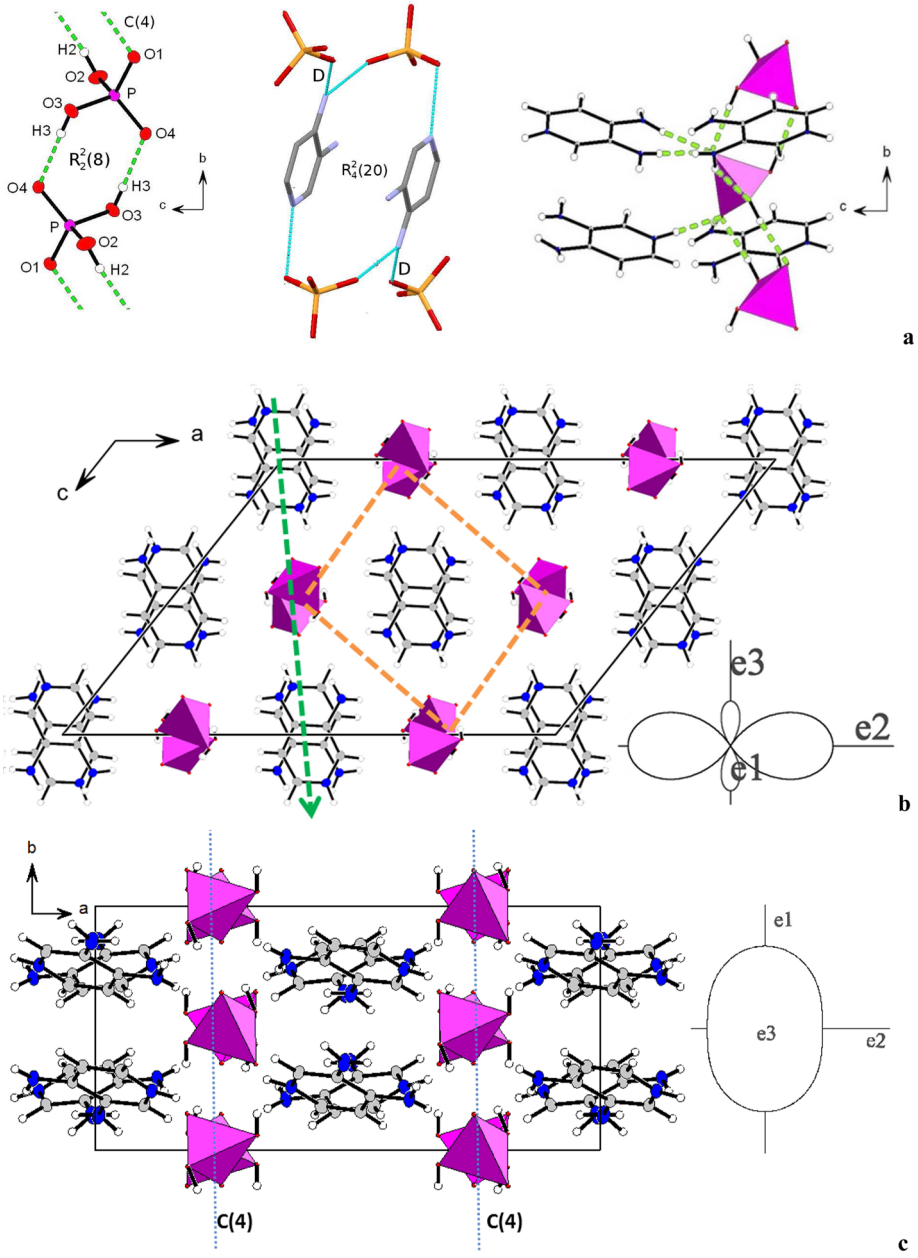

Figure 4. (a) Hydrogen bonds in the crystal structure. Left-hand side: O−H···O hydrogen bond between dihydrogen phosphate anions forming a cyclic dimer $R_2^2(8)$ and infinite C(4) chains of hydrogen bonds giving rise to the macroanion $(H_2PO_4)\infty$ (see text). Center: strong N−H···O hydrogen bonds between the organic cations and the dihydrogen phosphate anions giving rise to tetramer $R_4^2(20)$ and dimer D (H atoms have been omitted). Right hand side: Various hydrogen bonds between the organic cations and the inorganic cations. (b) Crystal packing of 3,4-diaminopyridine dihydrogen phosphate in the *ac* plane. The orange dotted line represents the four C(4) chains surrounding the central column with antiparallel 3,4-$DAPH^+$. Inset: Orientation of the thermal expansion tensor in the crystal. The eigenvector **e1** corresponds to the *b* axis (perpendicular to the picture); the eigenvectors **e2** and **e3** are in the *ac* plane. The thermal expansion along **e3** is negative. Anions and cations form infinite chains along the **e3** direction represented by a green dotted line. (c) Crystal packing of 3,4-diaminopyridine dihydrogen phosphate in the *ab* plane showing the infinite C(4) chains of dihydrogen phosphate anions $(H_2PO_4)\infty$ along the *b* axis linked by bridging 3,4-$DAPH^+$ (blue dotted line). Inset: Orientation of the thermal expansion tensor in the *ab* plane.

very strong because the corresponding O···O distance (2.640(2) and 2.582(2) Å) is of the same order of magnitude as the O···O distance within the $H_2PO_4^-$ tetrahedron itself. Moreover, the short P···P distance (4.078(2) Å) along those chains indicates that the infinite chain can be considered as a single polyanion, and they are sometimes called macroanions with the assignment $(H_2PO_4)\infty$.[43−46]

Each organic cation is connected by three strong N−H···O hydrogen bonds ($R^2_4(20)$ and D, see Figure 4a) to three different $(H_2PO_4)\infty$ inorganic chains. They bridge the chains in such a way that each column of antiparallel 3,4-$DAPH^+$ cations is surrounded by four different $(H_2PO_4)\infty$ inorganic chains (Figure 4b). The bridging N−H···O hydrogen bond is weaker than O−H···O hydrogen bond linking the phosphate moieties because the corresponding N···O distances range between 2.730(2) and 3.302(3) Å (Table 2). The organic cations are also involved in two additional N−H···O hydrogen bonds with the inorganic species, these hydrogen bonds are

dx.doi.org/10.1021/cg3014249 | *Cryst. Growth Des.* 2013, 13, 708−715

Table 2. Hydrogen Bonds of 3,4-Diaminopyridine Dihydrogen Phosphate at 296 K

D−H···A	d(D−H) (Å)	d(H···A) (Å)	d(D···A) (Å)	angle (D−H···A) (deg)
N1−H1A···O1	0.91(2)	1.82(2)	2.730(2)	175(3)
O2−H2···O1[a]	0.84(2)	1.80(2)	2.640(2)	175(2)
N2−H2A···O4[b]	0.89(2)	2.02(2)	2.908(2)	172(2)
N2−H2B···O1[c]	0.88(3)	2.08(3)	2.937(2)	165(2)
O3−H3···O4[d]	0.77(2)	1.81(2)	2.582(2)	178(3)
N3−H3A···O2[e]	0.92(4)	2.46(3)	3.302(3)	152(2)
N3−H3B···O4[b]	0.79(3)	2.38(3)	3.167(2)	174(3)
C1−H1···O2[e]	0.97(3)	2.58(2)	3.405(3)	143.7(15)
C4−H4···O3[c]	0.96(3)	2.49(3)	3.450(3)	178.2(13)

[a] $1/2 - x, 1/2 - y, 1 - z$. [b] $-x, -y, -z$. [c] $-1/2 + x, 1/2 - y, -1/2 + z$. [d] $1/2 - x, -1/2 - y, 1 - z$. [e] $x, -y, -1/2 + z$.

weaker than the others because the corresponding N−H···O angle is about 10° smaller (Figure 4a, Table 2).

Each dihydrogen phosphate ion is involved in three strong hydrogen bonds to three different 3,4-DAPH$^+$ cations. This gives rise to an infinite chain of interchanging anions and cations approximately along the [103] direction (Figure 4b). Finally, much weaker C−H···O interactions (Table 2) exist between the pyridine ring and the phosphate that have been observed by Le Bail and Smrčok too.[20]

X-ray Powder Diffraction As a Function of Temperature. High-resolution X-ray powder diffraction as a function of temperature from 160 K up to 400 K, near the melting point, gave rise to a single pattern matching the calculated pattern from the single crystal data and indicating the absence of any phase transition.

A Lebail fit to the data (see Figure 5) performed with the FullProf program[47] led to the lattice parameters compiled in

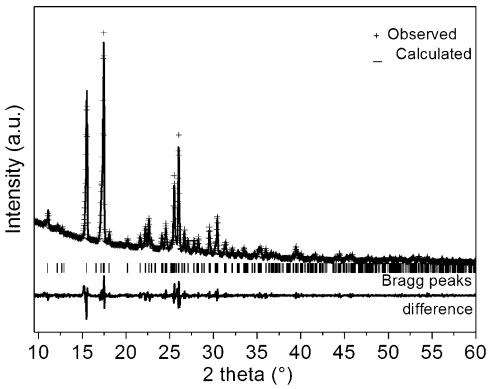

Figure 5. X-ray powder diffraction pattern recorded at 350 K compared to the pattern calculated by the LeBail fit. Below the fit of the data, the difference between the calculated and the observed intensity can be found. The goodness of fit is 4.25.

Table 3. The thermal expansion tensor has been calculated with the DEFORM software;[48] the eigenvalues, the eigenvectors, and the aspherism coefficient are compiled in Table 3. A graphical representation of the tensor at 310 K can be found in Figure 6. Projections of the tensor in the *ac* plane and *ab* plane are drawn in Figure 4b,c.

The aspherism coefficient varies from 0.4 to 0.7 between 160 and 400 K, indicating that the thermal expansion is anisotropic over the entire measurement range (Figures 4 and 6). The thermal expansion along **e3** is negative and smaller in absolute values than the expansion along **e1** and **e2**; thus, globally, the volume increases with the temperature (Table 3). The contraction along **e3** corresponds to an increase of β and a small decrease of the cell parameter c (Table 3). **e3** corresponds approximately to the direction [103]; that is the direction of the infinite chains of interchanging cations and anions (Figure 4b).

Crystal Morphology. There is an increasing interest in the structure, related properties, and reactivity of organic crystal surfaces. These surfaces are two-dimensional arrays where specific functional groups are exposed. The surface properties of the dominant crystal faces will be governed by those functional groups and even though they may not control solubility, which is a bulk property, solubilization is very much a function of favorable interactions between the solvent and the surface of the crystals. Knowledge of the surface structure at a molecular level is therefore important to control bioavailability of crystalline pharmaceutical solids.

The Miller indices of the prominent faces of the measured single crystal have been indexed directly on the diffractometer. The crystal is a polyhedron with 8 facets (Figure 6). The main flat facets were indexed as (001), (00$\bar{1}$), (201), ($\bar{2}$01), and ($\bar{1}$01). The longest edge of the crystal coincides with the b axis, the shortest crystallographic axis, as is generally the case.[51] It is the direction of the infinite chains of dihydrogen phosphate (Figure 6) and the direction of the largest thermal expansion in the crystal.

The 4 main facets (20$\bar{1}$), ($\bar{2}$01), (001), and (00$\bar{1}$) coincide with the planes defined by **e1**−**e3** and **e1**−**e2**, respectively. At these surfaces, the macroanion chains and the NH_2 moieties of the organic cations are located (see Figure S1 of Supporting Information). As both entities are polar, the surfaces are expected to be relatively hydrophilic and to possess high wettability for water.

Comparison with Structures of Other 3,4-DAPH$^+$ Salts. Comparing the different salts of 3,4-DAPH$^+$, it can be seen that the space group varies from triclinic (4-nitro-benzoate-4-nitrobenzoic acid) to orthorhombic (hydrogen tartrate) and that Z varies from 2 (hydrogen succinate and 4-nitro-benzoate-4-nitrobenzoic acid) to 8 (dihydrogen phosphate).

The packing of the hydrogen tartrate salt (hydrate) is similar to the packing of the dihydrogen phosphate salt; hydrogen tartrate anions and water molecules form infinite planes through strong hydrogen bonds. The plane comprises the crystallographic c axis (Figure 7).[16] Each 3,4-DAPH$^+$ cation is involved in 3 hydrogen bonds with 3 different water molecules or counterions.[16] There are $\pi\cdots\pi$ interactions between antiparallel 3,4-DAPH$^+$ ions, and all the organic cations are stacked in columns surrounded by water and counterions (Figure 7). The two main differences of the hydrogen tartrate packing are that all the aromatic rings of the organic cations are parallel[16] and that the distance between the columns is greater (9.42 instead of 7.21 Å in the dihydrogen phosphate salt).

The packing of the hydrogen squarate salt is different from that of the dihydrogen phosphate salt; each 3,4-DAPH$^+$ ion of the former is involved in three hydrogen bonds with three different counterions, and there are $\pi\cdots\pi$ interactions between antiparallel 3,4-DAPH$^+$ ions, but there are no infinite chains of counterions and no columns of antiparallel 3,4-DAPH$^+$ ions.[13]

The packings of the hydrogen succinate, the 2-carboxy-4,6-dinitrophenolate, and the 4-nitro-benzoate-4-nitrobenzoic acid salts are even more different; $\pi\cdots\pi$ interactions between antiparallel 3,4 DAPH$^+$ ions do not exist. The bonding scheme

dx.doi.org/10.1021/cg3014249 | Cryst. Growth Des. 2013, 13, 708−715

Table 3. Cell Parameters *a*, *b*, *c*, and *β*, Volume *V*, Thermal Expansion Tensor Eigenvalues α_{11}, α_{22}, and α_{33}, and Aspherism Coefficient *A* As a Function of the Temperature *T*

T (K)	*a* (Å)	*b* (Å)	*c* (Å)	*β* (deg)	*V* (Å^3)	$\alpha_{11}{}^a$ (K^{-1}) (10^{-4})	$\alpha_{22}{}^a$ (K^{-1}) (10^{-4})	$\alpha_{33}{}^a$ (K^{-1}) (10^{-4})	*A*
160	20.363(1)	7.7047(3)	14.639(1)	128.449(3)	1798.8(2)	0.4783	0.2600	−0.0250	0.408
220	20.395(1)	7.7199(3)	14.639(1)	128.466(3)	1804.7(2)	0.4770	0.2697	−0.0698	0.471
280	20.426(1)	7.7383(4)	14.638(1)	128.494(3)	1810.8(2)	0.4756	0.2818	−0.1172	0.545
310	20.442(1)	7.7490(3)	14.637(1)	128.508(3)	1814.4(2)	0.4749	0.2884	−0.1417	0.587
350	20.464(1)	7.7671(4)	14.633(1)	128.540(3)	1819.2(2)	0.4741	0.2977	−0.1747	0.649
400	20.4970(1)	7.7949(4)	14.6298(3)	128.594(3)	1826.8(2)	0.4729	0.3099	−0.2167	0.735

[a]Eigenvalues of the corresponding eigenvectors (**e1**, **e2**, and **e3**) at 310 K in the unit cell: **e1** = 0.129 × *b*; **e2** = 0.054 × *a* + 0.013 × *c*; **e3** = −0.031 × *a* − 0.09 × *c*.

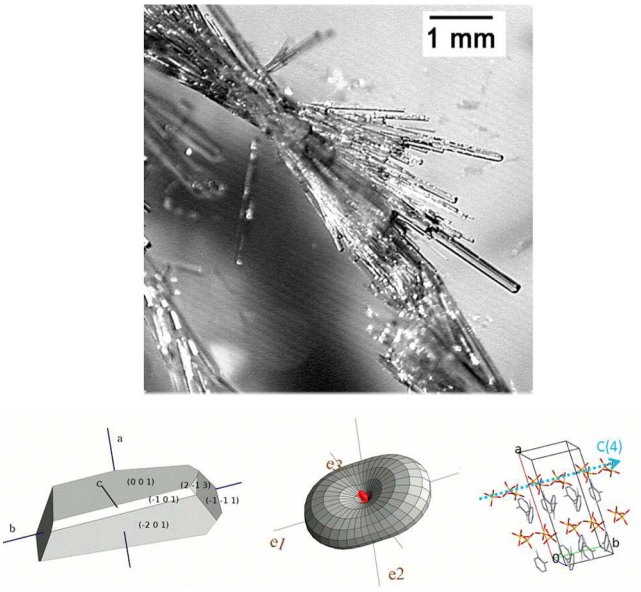

Figure 6. Optical microscopy photograph of 3,4-diaminopyridine dihydrogen phosphate crystals. Thermal expansion tensor at 310 K drawn with WinTensor on the basis of its eigenvectors **e1**, **e2**, and **e3** (red indicates negative expansion).[49] Experimental morphology of the measured single crystal (drawing with WinXmorph[50]), compared to the thermal expansion tensor and the crystal structure (H atoms are omitted).

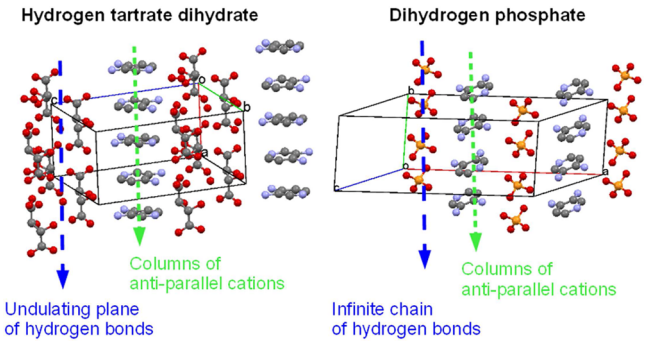

Figure 7. Comparison between the packing of the hydrogen tartrate salt[16] (left) and the dihydrogen phosphate salt (right); in both cases, there are columns of antiparallel cations along the vertical axis of the figure. The cations are connected by strong hydrogen bonds to the surrounding anions.

is very different, too. In the hydrogen succinate salt, each 3,4-DAPH$^+$ is involved in five hydrogen bonds with five different counterions. In the 4-nitro-benzoate-4-nitrobenzoic acid salt, the position of the counterion is disordered.[12]

In Figures 8 and S2 (Supporting Information), the 2D fingerprint plots of the Hirshfeld surfaces calculated from the crystal structures can be found. The similarities between the packings have been discussed above, but the Hirshfeld surfaces provide an analysis of the environment of the molecules from a different point of view. The most striking aspect of these fingerprint plots is their similarity. Indeed, in all the structures of the 3,4-DAPH$^+$ salts, the longest spike reflecting the shortest contacts (Figure 8 and S2, Supporting Information) is due to the O···H hydrogen bonds between the organic cation and the inorganic anions. 2-Carboxy-4,6-dinitrophenolate exhibits disorder of the counterion,[12] and this can be observed using a fingerprint plot; one of the two disordered counterion positions, however, demonstrates a clear similarity with the other structures as can be seen in Figure S2, Supporting Information.

The similarity between the fingerprint plots indicates that the intermolecular interactions in all the crystal structures is similar. Indeed, in all the structures, the 3,4-DAPH$^+$ cation is the hydrogen bond donor, and the counterion, the acceptor. Only the tartrate salt shows an additional sharp spike close to the main spike, due to the water molecules in the crystal structure, which are also hydrogen bond acceptors. In addition, it can be observed that the strong hydrogen bonds in the squarate and 4-nitro-benzoate-4-nitrobenzoic acid salts are slightly longer than in the other salts (higher d_e/d_i values). In Figure S3 of the Supporting Information, the relative occurrence of the different molecular interactions can be found.

CONCLUSIONS

The crystal structure of 3,4-diaminopyridine dihydrogen phosphate has been obtained at room temperature in combination with its thermal expansion. It confirms the structure previously solved from high-resolution powder diffraction, and it improves the resolution of the structure. In particular, this work shows that one hydrogen atom from the phosphoric acid is linked to the nitrogen atom of the pyridine ring. Thus, phosphoric acid does not appear to be strong enough to ionize a second N-atom from one of the NH_2 groups as perchloric acid does.[19] The crystal morphology has been studied, and the packing modes adopted by the 3,4-DAPH$^+$ cations in six different salts have been compared. The molecular packings of the hydrogen tartrate and the dihydrogen phosphate salts possess strong similarities; the 3,4-DAPH$^+$ ions are located in columns and between the cations in the column antiparallel $\pi\cdots\pi$ interactions exist. The fingerprint plots exhibit subtle differences between the two structures that are mainly due to the presence of water molecules in the tartrate salt. Interestingly, these two salts that demonstrate

dx.doi.org/10.1021/cg3014249 | Cryst. Growth Des. 2013, 13, 708−715

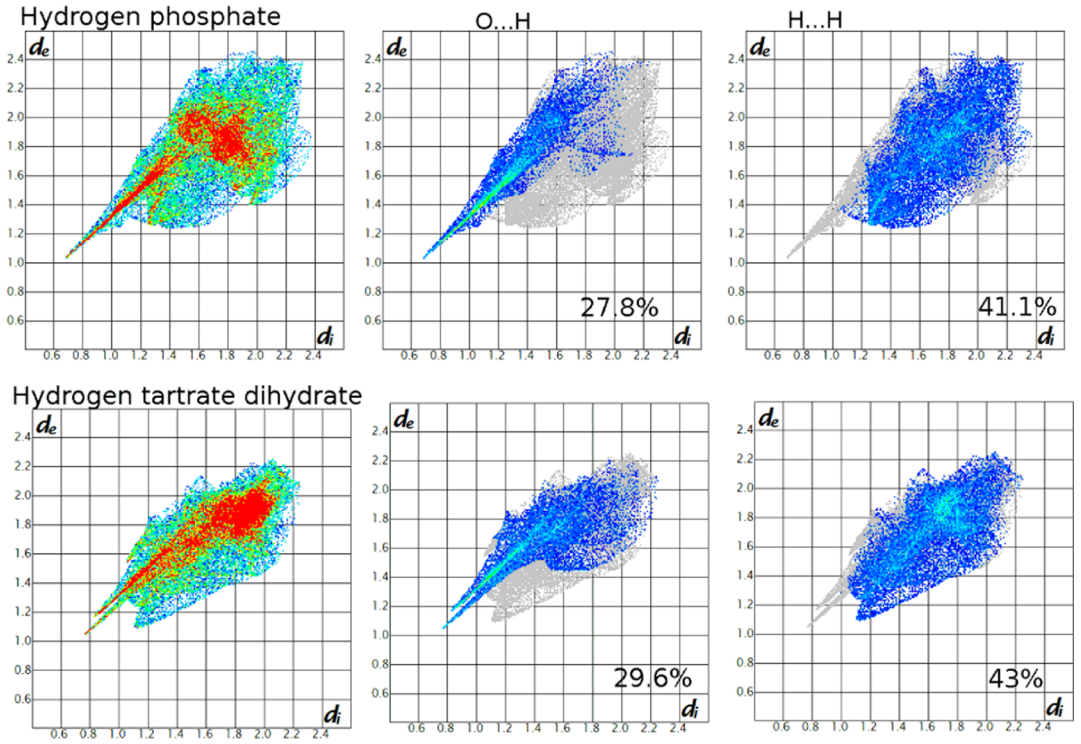

Figure 8. Fingerprint plots of 3,4-DAPH$^+$ in the dihydrogen phosphate and the tartrate salts and resolved into O···H and H···H contacts showing the percentages of contacts contributing to the total of the Hirshfeld surface area.

equivalent crystal structures have been selected for therapeutic use because of their physical properties.

The measurement of the thermal expansion has led to a new case of uniaxial negative thermal expansion, which so far has appeared to be very rare. The strongest thermal expansion coincides with an infinite hydrogen bonded chain of anions running parallel to the main axis of the crystalline rods. The negative thermal expansion is observed along an interchanging chain of anions and cations perpendicular to the main axis of the crystals.

■ ASSOCIATED CONTENT

Supporting Information

Table S1, selected geometric parameters of the structure of 3,4-DAP; Figure S1, surface structure of face $(20\bar{1})$ and (001); Figure S2, fingerprint plots of 3,4-DAPH$^+$ in different salts; Figure S3, relative contributions of the intermolecular interactions to the structures of the different salts; Unit cell interconversion between the present unit cell and that of ref 20; Figure S4, overlay of the two crystal systems; Figure S5, relative position of the two unit cells; CIF file of the crystal structure of 3,4-diaminopyridine dihydrogen phosphate. This material is available free of charge via the Internet at http://pubs.acs.org.

■ AUTHOR INFORMATION

Corresponding Author

*Tel: +33 1 53739675. E-mail: ivo.rietveld@parisdescartes.fr.

Notes

The authors declare no competing financial interest.

■ ACKNOWLEDGMENTS

We thank François Michaud of the Service Commun d'Analyse par Diffraction des Rayons X, Université de Bretagne Occidentale, France, for obtaining the single crystal data. We also thank Sanofi-Aventis for sustained financial support. M.B. and J.-Ll.T. were supported by the Spanish Ministry of Science and Innovation (Grant FIS2011- 24439) and the Catalan Government (Grant 2009SGR-1251).

■ REFERENCES

(1) Lambert, E. H.; Eaton, L. M.; Rooke, E. D. *Am. J. Physiol.* **1956**, *187*, 612−613.
(2) Murray, N. M. F.; Newsom-Davis, J. *Neurology* **1981**, *31* (3), 265−271.
(3) Sanders, D. B.; Massey, J. M.; Sanders, L. L.; Edwards, L. J. *Neurology* **2000**, *54* (3), 603−607.
(4) McEvoy, K. M.; Windebank, A. J.; Daube, J. R.; Low, P. A. *N. Engl. J. Med.* **1989**, *321* (23), 1567−1571.
(5) Judge, S. I.; Bever, C. T. *Pharmacol. Ther.* **2006**, *111* (1), 224−259.
(6) Guyon, F.; Pradeau, D.; Le Hoang, M. D.; Houri, J.-J. Tartrate et phosphate de 3,4-diaminopyridine, compositions pharmaceutiques et utilisations. EP 1 358 159 B1, 2009.
(7) Goulay-Dugay, S. Contibution au développement analytique et bioanalytique d'une substance active utilisée dans le traitement d'une maladie rare. Ph.D. thesis, Université Paris Descartes, Paris, France, 2009.
(8) Gould, P. L. *Int. J. Pharm.* **1986**, *33* (1−3), 201−217.
(9) Raust, J. A.; Goulay-Dufay, S.; Le Hoang, M. D.; Pradeau, D.; Guyon, F.; Do, B. *J. Pharm. Biomed. Anal.* **2007**, *43* (1), 83−88.
(10) Datta, S.; Grant, D. J. *Nat. Rev. Drug Discovery* **2004**, *3* (1), 42−57.
(11) Rubin-Preminger, J. M.; Englert, U. *Acta Crystallogr., Sect. E* **2007**, *63*, O757−O758.
(12) Hemamalini, M.; Fun, H.-K. *Acta Crystallogr., Sect. E* **2010**, *66*, O2747−U1973.
(13) Koleva, B.; Tsanev, T.; Kolev, T.; Mayer-Figge, H.; Sheldrick, W. S. *Acta Crystallogr., Sect. E* **2007**, *63*, O3356−U2030.
(14) Fun, H.-K.; Balasubramani, K. *Acta Crystallogr., Sect. E* **2009**, *65*, 01531−U2099.

(15) Fun, H.-K.; Balasubramani, K. *Acta Crystallogr., Sect. E* **2009**, *65*, O1887−U3226.
(16) Koleva, B. B.; Kolev, T.; Tsanev, T.; Kotov, S.; Mayer-Figge, H.; Seidel, R. W.; Sheldrick, W. S. *J. Mol. Struct.* **2008**, *881* (1−3), 146−155.
(17) Qin, J.-H.; Wang, J.-G. *Acta Crystallogr., Sect. E* **2009**, *65*, O131−U2400.
(18) Hemamalini, M.; Fun, H.-K. *Acta Crystallogr., Sect. E* **2010**, *66*, O639−U5226.
(19) Koleva, B. B.; Kolev, T.; Tsanev, T.; Kotov, S.; Mayer-Figge, H.; Seidel, R. W.; Sheldrick, W. S. *Struct. Chem.* **2008**, *19* (1), 13−20.
(20) Le Bail, A.; Smrcok, L. *Powder Diffr.* **2011**, *26* (4), 321−325.
(21) Oxford-Diffraction. *CrysAlis*, 2005.
(22) Sheldrick, G. M. *Acta Crystallogr., Sect. A: Found. Crystallogr.* **2008**, *64*, 112−122.
(23) Spek, A. L. *Acta Crystallogr., Sect. D. Biol. Crystallogr.* **2009**, *65*, 148−155.
(24) Salud, J.; Barrio, M.; Lopez, D. O.; Tamarit, J. L.; Alcobe, X. *J. Appl. Crystallogr.* **1998**, *31*, 748−757.
(25) Chanh, N. B.; Clastre, J.; Gaultier, J.; Haget, Y.; Meresse, A.; Lajzerowicz, J.; Filhol, A.; Thomas, M. *J. Appl. Crystallogr.* **1988**, *21*, 10−14.
(26) Negrier, P.; Pardo, L. C.; Salud, J.; Tamarit, J. L.; Barrio, M.; Lopez, D. O.; Wurflinger, A.; Mondieig, D. *Chem. Mater.* **2002**, *14* (5), 1921−1929.
(27) Parat, B.; Pardo, L. C.; Barrio, M.; Tamarit, J. L.; Negrier, P.; Salud, J.; Lopez, D. O.; Mondieig, D. *Chem. Mater.* **2005**, *17* (13), 3359−3365.
(28) Nicolai, B.; Mahe, N.; Ceolin, R.; Rietveld, I. B.; Barrio, M.; Tamarit, J.-L. *Struct. Chem.* **2011**, *22* (3), 649−659.
(29) Fortes, A. D.; Wood, I. G.; Knight, K. S. *Phys. Chem. Miner.* **2008**, *35* (4), 207−221.
(30) Negrier, P.; Barrio, M.; Tamarit, J. L.; Veglio, N.; Mondieig, D. *Cryst. Growth Des.* **2010**, *10* (6), 2793−2800.
(31) Weigel, D.; Beguemsi, T.; Garnier, P.; Berar, J. F. *J. Solid State Chem.* **1978**, *23* (3−4), 241−251.
(32) Parkin, A.; Barr, G.; Dong, W.; Gilmore, C. J.; Jayatilaka, D.; McKinnon, J. J.; Spackman, M. A.; Wilson, C. C. *CrystEngComm* **2007**, *9* (8), 648−652.
(33) Braun, D. E.; Gelbrich, T.; Kahlenberg, V.; Tessadri, R.; Wieser, J.; Griesser, U. J. *Cryst. Growth Des.* **2009**, *9* (2), 1054−1065.
(34) Wolff, S. K.; Grimwood, D. J.; McKinnon, J. J.; Jayatilaka, D.; Spackman, M. A. *CrystalExplorer 2.1*, 2007.
(35) Spackman, M. A.; Jayatilaka, D. *CrystEngComm* **2009**, *11* (1), 19−32.
(36) Spackman, M. A.; McKinnon, J. J.; Jayatilaka, D. *CrystEngComm* **2008**, *10* (4), 377−388.
(37) Spackman, M. A.; McKinnon, J. J. *CrystEngComm* **2002**, *4*, 378−392.
(38) Grabowsky, S.; Dean, P. M.; Skelton, B. W.; Sobolev, A. N.; Spackman, M. A.; White, A. H. *CrystEngComm* **2012**, *14* (3), 1083−1093.
(39) Karpagam, J.; Sundaraganesan, N.; Kalaichelvan, S.; Sebastian, S. *Spectrochim. Acta, Part A* **2010**, *76* (5), 502−512.
(40) Dwivedi, A.; Siddiqui, S. A.; Misra, N.; Raj, K.; Prasad, O.; Sinha, L.; Misra, N. *Pharm. Chem.* **2009**, *1* (2), 258−268.
(41) Demir, S.; Yilmaz, V. T.; Harrison, W. T. A. *Acta Crystallogr., Sect. C: Cryst. Struct. Commun.* **2005**, *61*, O565−O567.
(42) Hamed, K.; Samah, A.; Mohamed, R. *Acta Crystallogr., Sect. E* **2007**, *63*, O2896−U2384.
(43) Khemiri, H.; Ben Nasr, C.; Rzaigui, M.; Brahim, K. *Phosphorus, Sulfur Silicon Relat. Elem.* **2007**, *182* (10), 2269−2282.
(44) Baouab, L.; Jouini, A. *J. Solid State Chem.* **1998**, *141* (2), 343−351.
(45) Czapla, Z.; Dacko, S.; Waskowska, A. *J. Phys.: Condens. Matter* **2003**, *15* (22), 3793−3803.
(46) Chtioui, A.; Benhamada, L.; Jouini, A. *Mater. Res. Bull.* **2005**, *40* (12), 2243−2255.
(47) Rodriguez-Carvajal, J. *FullProf (Software)*, 2.0; 2000.
(48) Filhol, A.; Lajzerowicz, J.; Thomas, M. *Deform*, 1987.
(49) Kaminski, W. *WinTensor*, version 1.1, 2004; see http://www.wintensor.com.
(50) Kaminsky, W. *WinXMorph*, version 1.0, 2007; see http://cad4.cpac.washington.edu/WinXMorphHome/WinXMorph.htm.
(51) Donnay, J. D. H.; Harker, D. *Am. Mineral.* **1937**, *22*, 446−467.